Permeability and Nanoparticle Filtration Assessment of Cordierite-Bonded Porous SiC Ceramics

Atanu Dey, Nijhuma Kayal, and Omprakash Chakrabarti*

Central Glass and Ceramic Research Institute, CSIR, Kolkata 700 032, West Bengal, India

Rafael F. Caldato, Caio M. André, and Murilo D. M. Innocentini

Course of Chemical Engineering, University of Ribeirão Preto (UNAERP), 14096-900 Ribeirão Preto, São Paulo, Brazil

ABSTRACT: Cordierite bonded porous SiC ceramics having pore fractions (ε) between 0.33 and 0.72 and pore sizes of 6−50 μm, flexural strength of 5−54 MPa, and elastic modulus of 6−42 GPa were prepared by oxide bonding at 1350 °C in air compacts of SiC, Al_2O_3 and MgO powders with petroleum coke (PC) as the sacrificial pore former. To test the applicability of the porous ceramics in the fluid flow field, air permeation behavior was studied with fluid superficial velocity from 0.083 to 0.90 m s^{-1} and at 26−750 °C. The Darcian, k_1, and the non-Darcian, k_2, permeability coefficients were evaluated by fitting Forchheimer's equation to the experimental results. The temperature dependence of the permeability coefficients was explained from structural changes occurring during test conditions. The collection efficiency of filter ceramics ($\varepsilon = 0.62−0.68$) operating on removal of nanosized aerosol particles with sizes varying from 7 to 300 nm was determined by counting particles before and after filtration at a fluid superficial velocity of 0.1 m s^{-1}. Experimental results showed variation of collection efficiency from 96.7 to 99.9%. The size-selective fractional collection efficiency at different porosity levels was derived by using the well-known single-collector efficiency model considering some boundary conditions, and the model data were validated with experimental results. The test results were used for examination of the applicability of the filter ceramics in nanoparticle filtration processes.

I. INTRODUCTION

Porous SiC ceramics are promising filtering media for the control of particulate matter (PM) emissions from off-gas streams in many important industrial processes, such as coal/biomass combustion and gasification for power generation, thermal remediation of contaminated soils, incineration of biomedical and industrial wastes, metal smelting, and manufacturing of cement, carbon black, and glass, etc.[1−11] The long-term needs of the power generation systems have driven the development of high-temperature particle filtration technology using ceramic filters, but the focus is now shifted more and more to the chemical and process industry. SiC ceramics have low bulk density, excellent mechanical and chemical stability, high thermal conductivity, and thermal shock resistance, and they can also withstand high temperatures and hostile atmospheres. Processing routes are found to retain or create porosity without sacrificing these special properties. Oxide bonding is one of the major techniques used for synthesis of porous SiC ceramics. This technique is simple and inexpensive because it does not require any sophisticated equipment and delicate instrumentation. SiC ceramics can be processed by the oxide bonding technique at low temperatures (1300−1550 °C) under an ambient atmosphere using commercial-grade raw powders. Clay, silica, and mullite are often used as oxide bonds for SiC.[12−17] Cordierite (2MgO·2Al$_2$O$_3$·5SiO$_2$) is also considered another important bond as it has a low thermal expansion coefficient and good thermal and chemical stability and can be processed at a low temperature (1350 °C).[18]

Studies on permeation behavior of porous ceramics are important as the results can be used to determine the optimum flow conditions and characteristic features of filtering media to ensure that the cost of fan shaft power (operational cost) and filtering media (capital cost) is kept to a minimum for effective off-gas cleaning. The face velocity and the pressure drop with which ceramic filters typically operate vary in the ranges of 1−5 cm s^{-1} and 100−8000 Pa, respectively, depending on the particle collection efficiency and the characteristic features (porosity, pore size, thickness, and structure type, e.g., granular, fibrous, and cellular, etc.) of the filtering medium.[2,11,19,20] For high flow rate exhaust gases that often occur in many industrial processes, optimization of filter structure causes the operational pressure drop to decrease and the face velocity to increase without any change in the overall collection efficiency, implying useful savings of power and space for filter installation and operation.

The impact on air quality of hot gas cleaning technologies is also an important issue that needs to be considered during development of ceramic filters. The collection efficiency of a filter depends on the PM emission limit and the PM concentration of a hot aerosol stream. For stringent environmental control, acceptable limits of airborne particles finer than 10 μm (PM 10) and 2.5 μm (PM 2.5) are regulated. With the rapid development of new technologies, new processes, and

new products based on nanoparticles, the knowledge on how these materials severely affect human health and life also grows very fast and serious considerations are being given on issues of bringing the emissions of ultrafine particles—particles finer than 0.1 μm (PM 0.1)—from industrial processes under stringent regulatory control.[21] The researchers, thus, now consider the size of airborne particles an important ultimate parameter of processing and optimization of industrial filters. Ceramic filters must have the ability to capture ultrafine dusts, meet the stringent PM emission standards, and perform in a way similar to high-efficiency particulate air (HEPA) filters or ultralow penetration air (ULPA) filters that exhibit size-selective performance in workplace and clean room applications.

In this context, the present study is performed as a part of an Indian–Brazilian research project that aims to develop high-performance SiC ceramic filters for removal of fine and ultrafine particulate matter from hot gas streams in industrial applications. The focus of this paper is on performance evaluation of cordierite bonded SiC filters processed by the oxide bonding technique. The influences of structural parameters (porosity and pore size) on mechanical and permeability characteristics were evaluated and discussed. Experimental data of nanoaerosol filtration by the porous ceramics were acquired and compared to the existing models in order to determine the best parameters for the optimized filter compositions.

II. EXPERIMENTAL PROCEDURE

(1). Sample Preparation. Powders of SiC (α-SiC; purity, 98.20% (w/w); d_{50} = 22.5 μm; Grindwell Norton Ltd., Mumbai, India), Al_2O_3 (α-Al_2O_3; purity > 98% (w/w); d_{50} = 6.5 μm; Indian Aluminum Co. Ltd., Bangalore, India), MgO (purity > 97% (w/w); d_{50} = 4.5 μm; Mark Specialties India Pvt. Ltd., Mumbai, India), and petroleum coke (ash content, 0.68% (w/w); d_{50} = 11.4 μm; Assam Carbon Products Ltd., Assam, India) as the pore former were taken in such a way that the weight ratio (R) of Al_2O_3 to MgO was 2.53, the ratio (y) of combined weight of Al_2O_3 and MgO to a total weight of Al_2O_3, MgO, and SiC was 0.20, and the volume fraction (x) of the pore former varied from 0.23 to 0.76. The powders were wet mixed in a suitable liquid medium, dried, and pressed in the form of bars ($47 \times 20 \times 13$ mm^3) and discs (40 mm diameter $\times$ 10 mm thickness). Well-dried bars and discs were fired at 1100 °C in air for 4 h in an electrically heated furnace (Model No.-TE-3499-2, Therelek Engineers (P) Ltd., Bangalore, India) for burning of the pore former and subsequently sintered at 1350 °C for 4 h to produce the cordierite bonded porous SiC ceramic samples.

(2). Sample Characterization. Apparent porosity of the sintered samples was measured by water immersion method. Identification of product phases was made by X-ray diffractometry technique (XRD, PW 1710, Philips, Eindhoven, The Netherlands, with Cu Kα radiation of the wavelength of 1.5406 Å). Microstructural examination was done by scanning electron microscopy (SEM, Model SE-440, Leo-Cambridge, Cambridge, U.K.). The average pore size and the pore size distribution were evaluated by Hg-intrusion porosimetry (Poremaster, Quantachrome Instruments Inc., Boynton Beach, Florida, USA). Room-temperature flexural strength was determined in the three-point mode (sample dimension, 45 $\times$ 4.7 $\times$ 3.5 mm^3; span, 40 mm; loading rate, 0.5 mm min^{-1}) in an Instron Universal Testing Machine (Model 1123, Instron

Corp., Norwood, MA, USA). Young's modulus was determined from the slope of the load-deflection curves using standard software (Instron Bluehill-2, Bucks, U.K.).

Permeability to air flow was evaluated from room temperature to around 750 °C using a laboratory-made air permeator described elsewhere.[22−25] Permeability coefficients of the samples (discs of 40 mm diameter and 10 mm thickness) were determined by the Forchheimer's equation applicable for the compressible flow of fluids through flat membranes:[26−29]

$$\frac{P_i^2 - P_o^2}{2P_oL} = \frac{\mu v_s}{k_1} + \frac{\rho v_s^2}{k_2} \tag{1}$$

where P_i and P_o are, respectively, the absolute air pressures at the entrance and exit of the sample, v_s is the outlet superficial air velocity, i.e., volumetric air flow rate at the sample exit (Q) divided by the cross-sectional area normal to the flow (A), L is the sample thickness, μ and ρ are respectively the viscosity and the density of the permeating fluid (air), and k_1 and k_2 are, respectively, the Darcian and non-Darcian permeability coefficients, in reference to Darcy's law. The parameters k_1 and k_2 are introduced to account for the viscous and inertial effects on the flow systems. They incorporate only the structural features of the porous medium and therefore are considered constant even if the fluid or the flow conditions change.

A dimensionless parameter, known as Forchheimer's number, is defined by the expression:

$$Fo = \frac{\rho v_s(k_1/k_2)}{\mu} \tag{2}$$

which makes it possible to rewrite Forchheimer's equation in the following form:

$$\frac{P_i^2 - P_o^2}{2P_oL} = \frac{\mu v_s}{k_1}[1 + Fo] \tag{3}$$

The percentage contributions of viscous and inertial losses on total pressure drop of a ceramic filter can thus be estimated by[27]

$$\text{viscous contribution/\%} = \frac{1}{1 + Fo} \tag{4}$$

$$\text{inertial contribution/\%} = \frac{Fo}{1 + Fo} \tag{5}$$

The permeability coefficients k_1 and k_2 were obtained by polynomial fitting of Forchheimer's equation (eq 1) to v_s and ΔP experimental data. The density and the viscosity of air at a temperature T_o and pressure P_o (atmospheric pressure at the laboratory location (95.46 kPa)) at the exit stream were determined following the procedure described in ref 27.

The filtration behavior of the porous ceramics was examined by conducting the dust collection efficiency test at room temperature using NaCl nanoparticles (standard particles used for airborne dust filtration tests) of density 2165 kg m^{-3} and size ranging from 7 to 300 nm. The details of the experimental setup and the procedure of the test were described elsewhere.[22] The filtration velocity was fixed at 0.10 m s^{-1}, and the average inlet dust concentration was 1700 μg m^{-3}. The fractional collection efficiency (E_{frac}) at any particle size (i) was determined from the ratio of the difference of the particle concentration at the inlet ($C_{inlet,i}$) and the outlet ($C_{outlet,i}$) to the

particle concentration at the inlet. The overall particle collection efficiency ($E_{overall}$) was computed by

$$E_{overall} = \frac{C_{inlet} - C_{outlet}}{C_{inlet}} \qquad (6)$$

where C_{inlet} and C_{outlet}, the total concentrations of particles (μg m^{-3}) at the inlet and outlet of the filter, respectively, are obtained by

$$C_{inlet} = \sum_{i=7\,nm}^{300\,nm} C_{inlet,i} \qquad (7)$$

$$C_{outlet} = \sum_{i=7\,nm}^{300\,nm} C_{outlet,i} \qquad (8)$$

III. RESULTS AND DISCUSSION

(1). Structural and Physical Characterization. Sintered samples exhibited neither surface cracks nor distortion of shape. Negligible changes (<1%) of major dimensions were noticed. The recorded variation of apparent porosity (ε) was from 30.1 ± 1.2 to 71.7 ± 2.6%. XRD analysis detected α-SiC, cordierite, and cristobalite as the main crystalline phases present in the sintered samples. The presence of a negligible quantity of Al_2O_3 was also detected. In the starting mixtures the amounts of Al_2O_3 and MgO were such that stoichiometric formation of cordierite was possible. During sintering, SiC oxidized, oxidation derived SiO_2 reacted with Al_2O_3 and MgO forming cordierite, and the residual SiO_2 finally converted to cristobalite.[18]

Results of XRD analysis indicated that the cordierite formation reaction was nearly complete. Microstructure examination of the sintered samples indicated formation of an open-cell pore morphology. A typical micrograph of a sintered sample is shown in Figure 1. SiC particles were seen to be bonded at the contacting regions. Energy dispersive X-ray (EDX) analysis of the bond phase showed that it contained Mg, Al, Si, and O atoms, indicating formation of an oxide bond with an average Mg:Al atom ratio (1:2), the same as that of the cordierite. The Si:O atom ratio was different from that of cordierite, likely because of the presence of silica in the bond
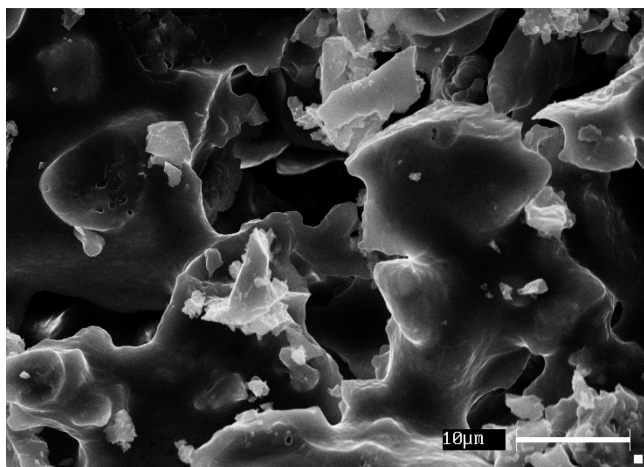
Figure 1. SEM image of cordierite bonded porous SiC ceramics synthesized from a powder compact having $x = 0.48$, $y = 0.20$, and $R = 2.53$.

phase. SiC particles were seen to be coated with a vitreous layer. At around 1350 °C formation of cordierite is accelerated due to crystallization of this phase directly from a liquid phase.[30] The SiC particles are likely to be coated with the liquid.

The porous SiC ceramics studied in the present work also behaved mechanically like cellular solids. The flexural strength of the porous ceramics varied within a range of 5.0 ± 0.8 to 53.7 ± 1.3 MPa, showing a trend for decreasing strength with increasing porosity (Figure 2). A similar trend was also
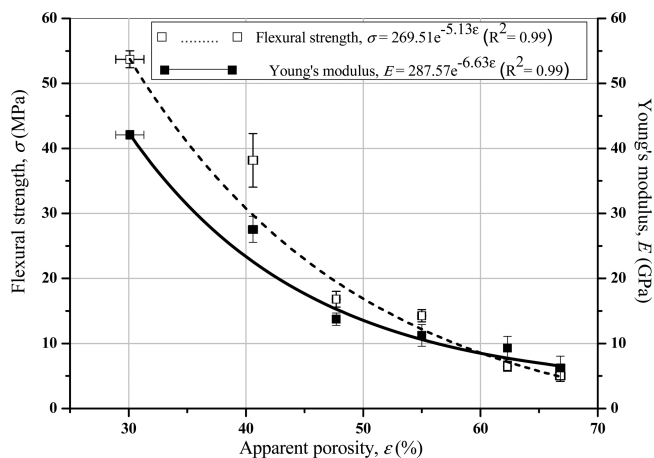
Figure 2. Flexural strength and elastic modulus of cordierite bonded porous SiC ceramics as a function of apparent porosity.

observed for elastic modulus (varied over the range of 6.2 ± 1.8 to 42.1 ± 6.8 GPa; Figure 2). These behaviors can be explained by the minimum solid area (MSA) based model that predicts an exponential relationship between porosity and mechanical property (strength (σ) or elastic modulus (E)) in cellular solids:[31,32]

$$\sigma = \sigma_o e^{-b\varepsilon} \qquad (9)$$

$$E = E_o e^{-b'\varepsilon} \qquad (10)$$

where σ and E are the flexural strength and elastic modulus of the material at a porosity level of ε and σ_o and E_o are the flexural strength and elastic modulus data of completely dense material; b and b' are constants that depend on the shape and stacking of the pores. The mechanical property and porosity data were well-fitted to eqs 11 and 12 (Figure 2), and the values of σ_o, b, E_o, and b' obtained from the fitting equations were 269 MPa, 5.1, 287 GPa, 6.6, respectively. The values of these constants obtained in the present work were in the ranges of the reported values.[13−15,33,34] The value of b can be 6 and 9 for cubic and rhombic stacking of pores.[35] The use of the rule of mixture further indicates that the stacking was predominantly cubic for the porous SiC ceramics investigated in the present work.

The average pore size (d_{pore}) increased from 5.6 to 49.5 μm, and the experimental d_{pore} and ε data were fitted to an exponential relation with a fairly good fitting quality (Figure 3). A porous medium bears a typical relation between d_{pore} and ε that depends on the very nature of the porous medium. For fibrous SiC ceramics synthesized by pressure-pulsed chemical vapor infiltration of carbonized cellulose powder performs, Ohzawa et al. observed that pore size varied with porosity in a nonlinear fashion.[36] Sepulveda et al. obtained a logarithmic
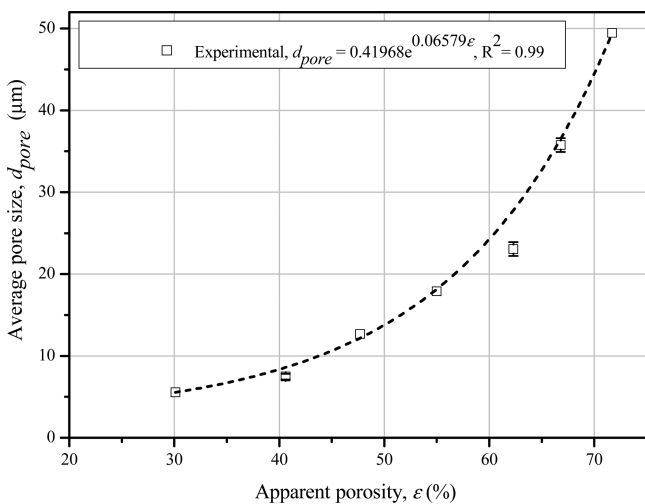
Figure 3. Dependence between average pore size and apparent porosity of SiC samples.

relationship between pore size and relative density (ρ_r) for highly porous hydroxyapatite synthesized by gel-casting of foams.[37] Since $\rho_r = 1 - \varepsilon$, the relation indicates that pore size changes with porosity in a logarithmic or exponential manner—a trend that was also obtained in the present work.

(2). Fluid Dynamic Characterization. The SiC samples of different porosities were tested for permeation initially with air flow under ambient conditions ($T_o \approx 29$ °C, $P_o \approx 95.06$ kPa; $\rho = 1.1$ kg m^{-3}; $\mu = 1.88 \times 10^{-5}$ Pa s). Experimental data and the respective model fitting curves are presented in Figure 4. The air velocity ranged from 0.083 to 0.67 m s^{-1}. The parabolic relationship between the pressure drop parameter $(P_i^2 - P_o^2)/2P_oL$ and superficial velocity (v_s) was confirmed through the high-quality fitting of Forchheimer's equation for compressible fluids (correlation coefficient $R^2 > 0.999$).

The permeability coefficients k_1 and k_2 were evaluated from the curves fitted to Forchheimer's equation in Figure 4. The data are presented in a comprehensive map proposed by Innocentini et al.[26,27] that classifies porous media according to
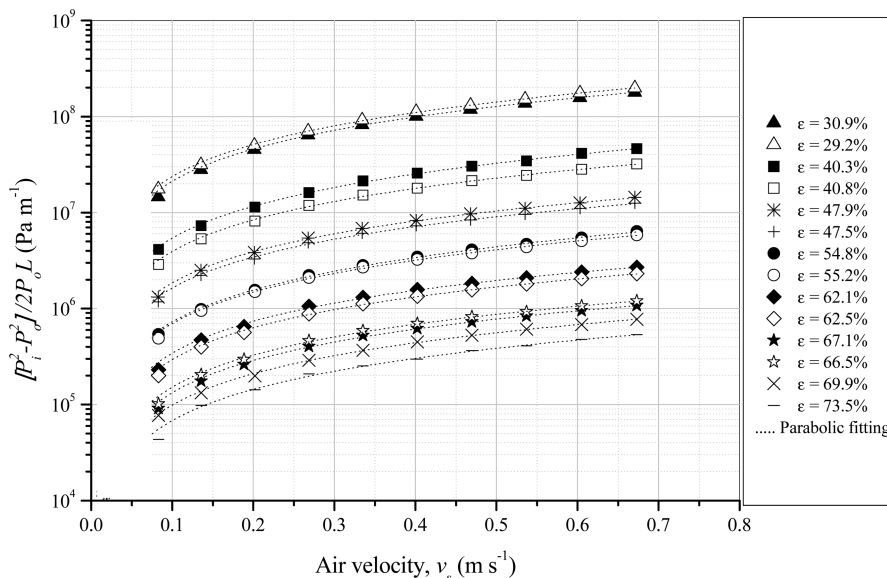
the type and application (Figure 5). Permeability of SiC porous samples was mostly located in the range for granular filters (k_1
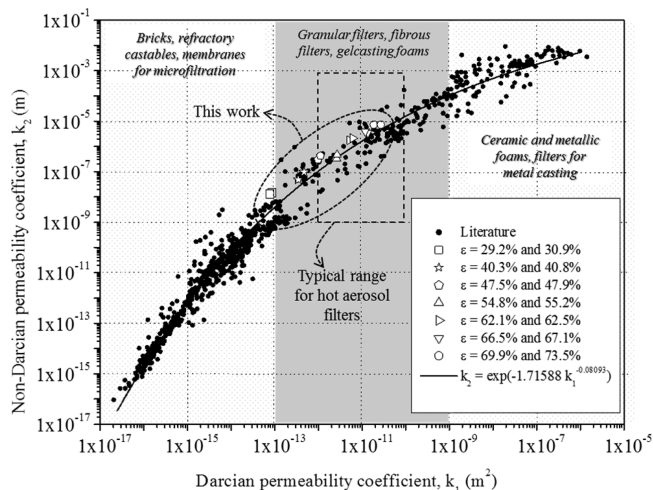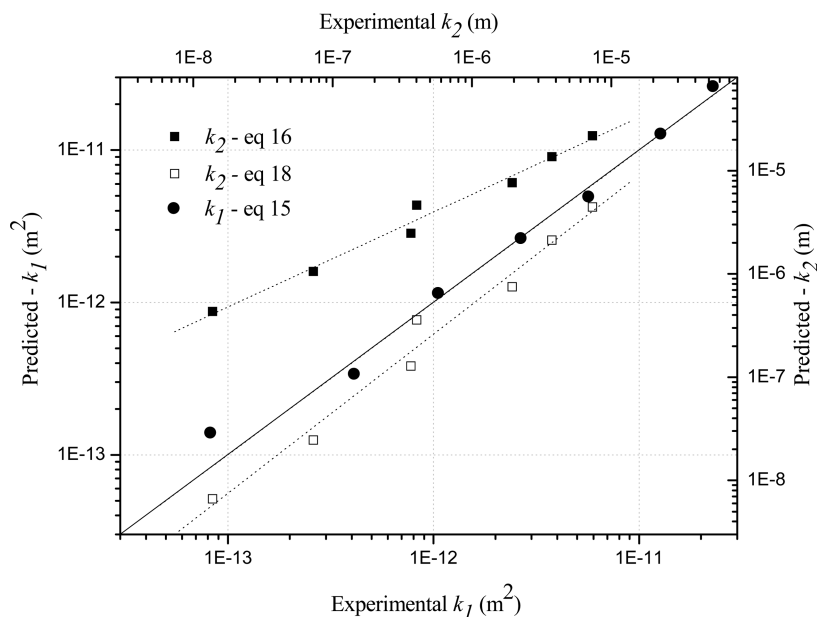

Figure 5. Classification of permeability data of cordierite based SiC filters tested in this work. (Adapted from Innocentini et al.[26,27])

$\approx 10^{-13}-10^{-15}$ m^2), corroborating literature data on ceramic filters.[19,27,38] A remarkable increase in permeability was achieved with the increase of porosity, and samples with $\varepsilon > 47.5\%$ were included in the typical range for hot aerosol filters as described in the literature.[19] The map is also useful for revealing an unequivocal relationship linking k_1 and k_2, regardless of the type of material. In cases in which only k_1 is available, k_2 can be fairly estimated by the expression:

$$k_2 = \exp\left(-\frac{1.71588}{k_1^{0.08093}}\right)$$

(11)

Permeability coefficients k_1 and k_2 are also usually related to porosity and to a characteristic length (d_{eq}) of the filter structure through Ergun-like equations, given by[27,39]

Figure 4. Permeation curves obtained with airflow at room temperature for samples of different porosities.

Experimental k_2 (m)

Figure 6. Comparison of theoretical prediction by Ergun-like equations and eq 18 of the present work and experimentally measured data of k_1 and k_2 (where, for example, 1E-11 represents 1×10^{-11}).

$$k_1 = \frac{d_{eq}^2 \varepsilon^3}{150(1-\varepsilon)^2} \quad (12)$$

$$k_2 = \frac{d_{eq}\varepsilon^3}{1.75(1-\varepsilon)} \quad (13)$$

For filters in which the solid matrix is continuous and the constitutive particles/grains/fibers are not individually recognizable, the average pore or cell size (d_{pore}) is considered as the characteristic length d_{eq}; on the other hand, if the filter is made of packed columns of loose multisided particles/grains/fibers, the characteristic length is customarily selected by the Sauter mean diameter (d_{vs}) of the particle/grain/fiber size distribution.[25] If the constitutive particles of the filter are spherical, then a simple relationship between d_{vs} and d_{pore} can be derived:[27]

$$d_{vs} = 1.5\frac{(1-\varepsilon)}{\varepsilon}d_{pore} \quad (14)$$

In this case, eqs 12 and 13 can be rewritten as

$$k_1 = \frac{2.25}{150}\varepsilon d_{pore}^2 \quad (15)$$

$$k_2 = \frac{1.5}{1.75}\varepsilon^2 d_{pore} \quad (16)$$

Equations 12 and 15 defining the Darcian coefficient k_1 have been tested and validated for a variety of unconsolidated porous media and also for several systems of partially sintered porous ceramics on the condition that the size distribution of ceramic raw materials is representative in the consolidated product. However, if the experimental data and studies in the literature are considered, one definite conclusion that can be drawn is that while Ergun equations work fine for k_1, they are not reliable for k_2 over a wide range of pore size or particle size, indicating that the Ergun approach does not fit the relationship between k_1 and k_2 well to the permeability map shown in Figure 5. This point is well-documented in the literature, as many

empirical equations have been suggested to predict k_2 based on the knowledge of k_1 obtained from Ergun equation (eqs 12 or 15).[40−43] One viable approach proposed in this work for estimation of k_2 from porosity and pore/particle size is based on the relationship between k_1 and k_2 derived from a large experimental data set, as shown in the permeability map of Figure 5, and is represented by eq 11. Substitution of Ergun equations for k_1—eqs 12 and 15—in eq 11 thus gives

$$k_2 = \exp\left(-\frac{2.57394(1-\varepsilon)^{0.16186}}{\varepsilon^{0.24279}d_p^{0.16186}}\right) \quad (17)$$

$$k_2 = \exp\left(-\frac{2.41044}{\varepsilon^{0.08093}d_{pore}^{0.16186}}\right) \quad (18)$$

To check the applicability of this approach, the experimental ε and d_{pore} data of SiC filters were used in eq 18 to estimate k_2, and the results were plotted in Figure 6, together with the values of k_2 predicted by Ergun eq 16 using the same ε and d_{pore} data. The $y = x$ line indicates the hypothetical agreement between predicted and experimental values obtained from the airflow tests. Plots in Figure 6 confirm that (i) as expected, Ergun eq 12 predicted very well the Darcian permeability k_1 for the sintered SiC filters of average pore size in the micrometric scale (from 5.6 to 45.5 μm) and a wide ranging porosity from 30.1 to 71.7%; (ii) Ergun eq 13 overestimated the non-Darcian coefficient k_2, and the deviation increased progressively with a decrease in k_1, also confirming the trends reported in the literature;[41] (iii) the proposed equation derived on the basis of the permeability map (eq 18) displayed a satisfactory and consistent predictability of k_2 in the entire range of experimental data.

Calculations based on experimental permeability coefficients k_1 and k_2 of samples of different porosities confirm that even for a relatively high face velocity of $v_s = 0.1$ m s^{-1}, the contributions of viscous effects and inertial effects to the total pressure drop shown by filter samples for air flow at 101.3 kPa and 30 °C are

97 and 3%, respectively. This proves that regardless of the porosity level, the airflow through porous SiC samples under typical ambient aerosol filtration conditions follows reasonably Darcy's law.

The influence of gas temperature on the permeation behavior of cordierite based SiC filters was investigated using samples of porosity at six different levels. Figure 7 illustrates typical
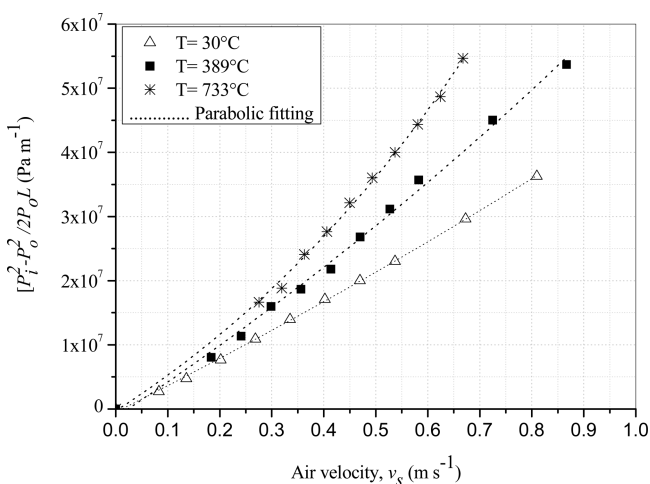
Figure 7. Typical permeation curves obtained for airflow in three temperature levels. Data presented are for a sample with porosity of 41.6%.

permeation curves for a sample of $\varepsilon = 41.6\%$ (airflow test was done with face velocity ranging from 0.083 to $\sim$0.90 m s^{-1} and at three temperatures). The results showed that the resistance to fluid flow increased with temperature, as reported by other authors.[25,44,45] The other samples tested under the same conditions also showed similar trends. The results also confirmed that the experimental data fitted to Forchheimer's equation (eq 1) exceptionally well.

The variations of permeability coefficients k_1 and k_2 with temperature for different samples are shown in Figure 8, which indicates a slight increase of k_1 and a decrease of k_2 with an increase of temperature from 30 to 750 °C. Similar qualitative trends were observed by Innocentini et al. for refractory
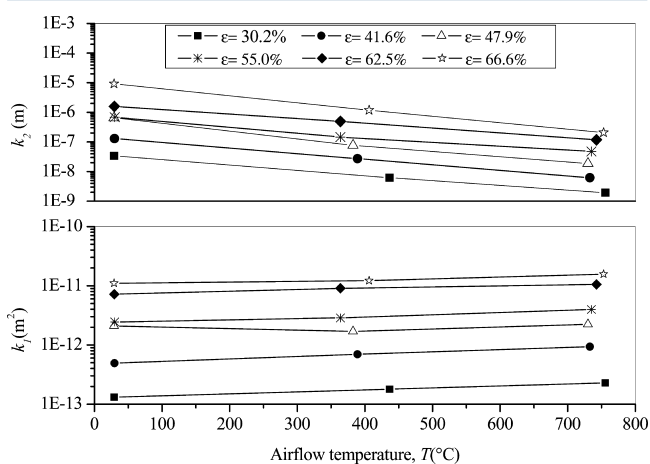
Figure 8. Influence of airflow temperature on permeability coefficients of cordierite bonded SiC samples of different porosity (where, for example, 1E-3 represents 1×10^{-3}).

castables,[23] by Barg et al. for freeze casting foams,[45] and by Biasetto et al. for porous lanthanum carbide discs.[25]

The permeation behavior of SiC filter samples (Figure 7) was thus affected not only by the changes of properties of air (increase of 131% in μ and decrease of 70% in ρ, for an increase of temperature from 30 to 750 °C) but also by the variation of permeability coefficients (average increase of 71% in k_1 and average decrease of 94% in k_2). All of these factors account for the change of pressure drop by the temperature. The situation can be better analyzed by the data generated on the basis of simulation of airflow through the SiC samples at $v_s = 0.05$ m s^{-1} and temperature at two levels (30 and 750 °C; Table 1). Equal sample thickness ($L = 0.01$ m) was considered. There are three aspects of the data presented in Table 1: (i) with temperature remaining the same, an increase in ε caused a clear reduction in filter pressure drop (ΔP); (ii) with porosity remaining constant, an increase in temperature caused the pressure drop to increase; (iii) the contribution of inertial effect on pressure drop was very small for all samples at 30 °C ($<$1.2%), and it was further reduced at 750 °C ($<$0.2%). Thus if it is considered that clean or virgin filtering elements are used at 300−1500 °C with $v_s = 0.05$ m s^{-1} and they show pressure drop values in the range of 1000−5000 Pa,[1] several conclusions can be drawn on the basis of the data shown in Table 1: (i) SiC samples of porosity >55% are the good candidates to be used as hot aerosol filters, as they exhibited pressure drop values comparable to those of commercial products; (ii) the increase of viscosity with temperature was the main factor responsible for the rising pressure drop levels of SiC filters; and (iii) at increasing airflow temperatures, tendencies of the pressure drop curves are to obey Darcy's law.[46]

(3). Dust Filtration Behavior. The mechanisms by which particles are arrested by filter media are well-documented in the published literature. The expressions were derived in the literature on the basis of semiempirical correlations, considering the process of filtration to be time-independent—a condition valid for the first stage of a filtration process when no dust cake is present in the filter. In the present work, the fractional collection efficiency of a filter in the first filtration stages was calculated using the single-collector efficiency model derived for granular filters:[47−49]

$$E_{frac} = 1 - \exp\left[-\frac{aKL(1 - \varepsilon)\eta_T}{d_c}\right] \quad (19)$$

where L, ε, and d_c represent respectively the filter thickness, filter porosity, and the average collector diameter (represented here as the average Sauter diameter of the raw SiC powder used to prepare the filter sample, d_{vs}); a is the fitting constant (in this work a is considered to be unity); and K is given by Yoshida and Tien as[49]

$$K = \left[\frac{6}{(1 - \varepsilon)^{2/3}}\right]^{1/3} \quad (20)$$

According to the model, the total collection efficiency of a single collector (η_T) is the combination of the individual contributions due to different collection mechanisms, diffusion (η_D), inertia (η_I), direct interception (η_{DI}), gravity (η_G), and electrophoresis (η_E). The single collector combined efficiency (η_T) is given by

Table 1. Pressure Drop Parameters Estimated by the Forchheimer's Equation for Airflow with $v_s = 0.05$ m s^{-1} through Samples of Different Porosities at Two Temperature Levels (30 and 750 °C)

	$T_o = 30$ °C			$T_o = 750$ °C			
ε (%)	ΔP (Pa)^a	$\Delta P_{viscous}$ (%)^b	$\Delta P_{inertial}$ (%)^c	ΔP (Pa)^a	$\Delta P_{viscous}$ (%)^b	$\Delta P_{inertial}$ (%)^c	$\Delta P_{increase: 30-750 °C}$ (%)
30.2	55911	98.8	1.2	98901	99.8	0.2	76.9
41.6	14750	98.8	1.2	24677	99.8	0.2	67.3
47.9	5740	99.0	1.0	10146	99.9	0.1	76.8
55.0	2963	98.9	1.1	5628	99.9	0.1	89.9
62.5	1144	98.6	1.4	2145	99.8	0.2	87.5
66.6	741	99.6	0.4	1430	100.0	0.0	93.0
66.7	343	99.1	0.9	673	99.9	0.1	96.2

^{a}Calculated by eq 1 using k_1 and k_2 from Figure 8, μ and ρ are as found in ref 27, and $L = 0.01$ m. ^{b}Calculated by eqs 2 and 4. ^{c}Calculated by eqs 2 and 5.

$$\eta_T = 1 - (1 - \eta_D)(1 - \eta_{DI})(1 - \eta_I)(1 - \eta_G)(1 - \eta_E) \tag{21}$$

The diffusional collection arises from the random movement of suspended small particles in a gas—known as Brownian diffusion—and the single-collector diffusional efficiency is given by[47]

$$\eta_D = 4(1 - \varepsilon)^{2/3} A_S^{1/3} N_{Pe}^{-2/3} \tag{22}$$

where the Happel's parameter (A_S) is given by

$$A_S = \frac{2(1 - (1 - \varepsilon)^{5/3})}{2 - 3(1 - \varepsilon)^{1/3} + (1 - \varepsilon)^{5/3} - (1 - \varepsilon)^2} \tag{23}$$

The Peclet number (N_{Pe}) and the diffusion coefficient (D) are given by

$$N_{Pe} = \frac{v_s d_{pi}}{D} \tag{24}$$

$$D = \frac{k_B T F_S}{3\pi\mu d_{pi}} \tag{25}$$

where d_{pi} is the nanoparticle dust size, k_B is the Boltzmann constant, T is the absolute temperature, μ is the air viscosity, and F_S is the slip correction factor which is given by Allen and Raabe as[50]

$$F_S = 1 + \frac{\lambda}{d_{pi}}\left[2.34 + 1.05 \exp\left(-0.39\frac{d_{pi}}{\lambda}\right)\right] \tag{26}$$

where λ is the mean free path of air. The single-collector inertia efficiency is given by[51]

$$\eta_I = 0.2589 N_{St,eff} N_R \tag{27}$$

The interception parameter (N_R) and the effective Stokes' number ($N_{St,eff}$) are

$$N_R = \frac{d_{pi}}{d_c} \tag{28}$$

$$N_{St,eff} = [A_S + 1.14 N_{Re}\varepsilon^{-1.5}]\frac{N_{St}}{2} \tag{29}$$

The Reynolds number (N_{Re}) and the Stokes' number (N_{St}) are given by

$$N_{Re} = \frac{\rho v_s d_c}{\mu} \tag{30}$$

$$N_{St} = \frac{\rho_p v_s F d_{pi}^2}{9\mu d_c} \tag{31}$$

The expression for estimation of the collection efficiency due to direct interception is given by[52]

$$\eta_{DI} = 6.3\varepsilon^{-2.4} N_R^2 \tag{32}$$

The collection efficiency due to gravitational effects is given by[52,53]

$$\eta_G = 3.75 \times 10^{-2}\left(\frac{v_t}{v_s}\right)^{0.5} \tag{33}$$

where the terminal settling velocity (v_t) of the dust particle is obtained within the Stokes free-fall regime ($N_{Re} < 1$) and g is the acceleration due to gravity.

$$v_t = \frac{\rho_p g d_{pi}^2}{18\mu} \tag{34}$$

The single-collector electrophoretic efficiency (η_E) was not considered in the present case as the NaCl dust particles were neutralized (by Kyrpton-85 Neutralizer) before they entered the filter.

Figure 9 presents the typical contribution of each mechanism to the total single-collector efficiency (η_T) in the size range of
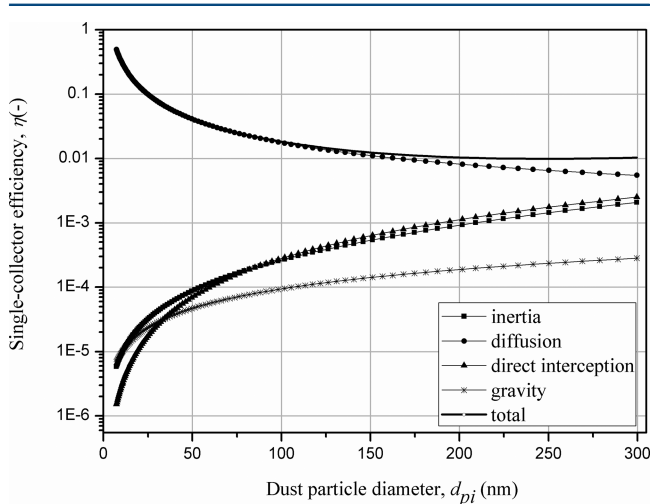
Figure 9. Contributions of different dust collection mechanisms to the single-collector efficiency for a filter with porosity of 68.42% (where, for example, 1E-3 represents 1×10^{-3}).

dust particles from 7 to 300 nm for the filter sample with porosity of 68.4%. Similar trends were also noticed for the other filter samples of different porosity.

The fractional filter efficiency (E_{frac}) was estimated as a function of dust particle size (d_{pi}) at different porosity levels by the sets of eqs 19−34 and using experimental conditions (mean free path of air at room temperature and atmospheric pressure: $\lambda = 7.56 \times 10^{-8}$ m; viscosity of air, $\mu = 1.86 \times 10^{-5}$ kg m^{-1} s^{-1}; density of air, $\rho = 1.08$ kg m^{-3}; and face velocity of aerosol, $v_s =$ 0.1 m s^{-1}). Figure 10 shows the plots correlating fractional efficiency with dust particle size.
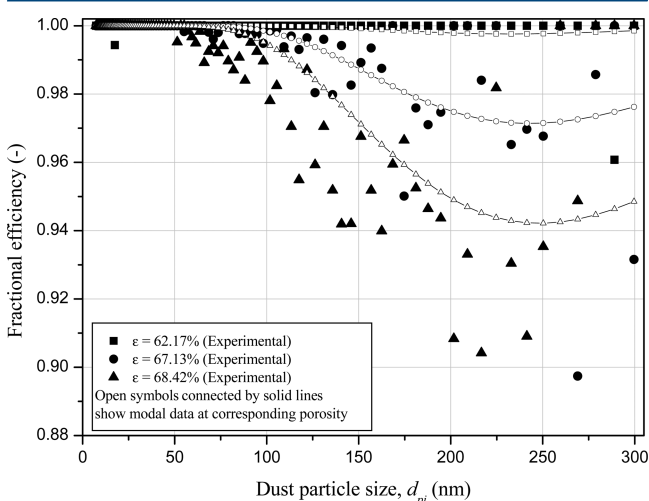
Figure 10. Comparison between modeling and experimental curves of fractional collection efficiency versus particle size at different levels of porosity of SiC filters.

At each porosity level the theoretical efficiencies also show a decreasing trend for larger particles up to 300 nm. A comparison between the modeling (theoretical) and experimental curves shows satisfactory agreement between the proposed correlation of fractional collection efficiency with particle size and the experimental results. The small differences that still exist between the modeling (theoretical) and the experimental curves may be due to the fact that calculations of fractional collection efficiencies are done on the basis of granular filter medium whereas the experiments were done using filters made of sintered porous ceramics. Figure 9 also reveals that the diffusional mechanism plays the most dominant role on the capture of nanoparticles by the filtering media. Other authors also indicated that Brownian diffusion is the most dominant dust collection mechanism for the capture of submicrometer size particles by fibrous filters.[54,55] The overall efficiency was found to decrease with porosity (Figure 10). The overall efficiency was also estimated using the single-collector model:

$$E_{overall} = \sum_{i=7\text{ nm}}^{300\text{ nm}} w_i E_{frac}$$

(35)

where E_{frac} is the fractional efficiency for the ith particle (eq 19) and w_i is the mass fraction:

$$w_i = \frac{C_{inlet,i}}{C_{inlet}}$$

(36)

The overall filter efficiency was estimated by eq 35. The accuracy of $E_{overall}$ depends on the proper fitting of the single-collector size in eq 19.

The dust collection efficiency test was conducted for samples with three levels of porosity (ε = 62.2, 67.1, and 68.4%). Table 2 shows that the model and the experimental overall efficiencies

Table 2. Comparison of the Predicted (Model) and Experimental Overall Efficiency, $E_{overall}$

	overall efficiency, E_{frac} (%)		fitting value of collector size, $d_c = d_{vs}$ (μm)
porosity (%)	experiment	model	
68.42	96.7	96.9	23.7
67.13	98.6	98.5	22.0
62.17	99.9	99.9	19.6

tally very well if the values of the single-collector size are selected from a range of 19.6−23.7 μm—a range of particle diameter with which the single-collector size agrees very well in the present study. Figure 11 shows a very good agreement
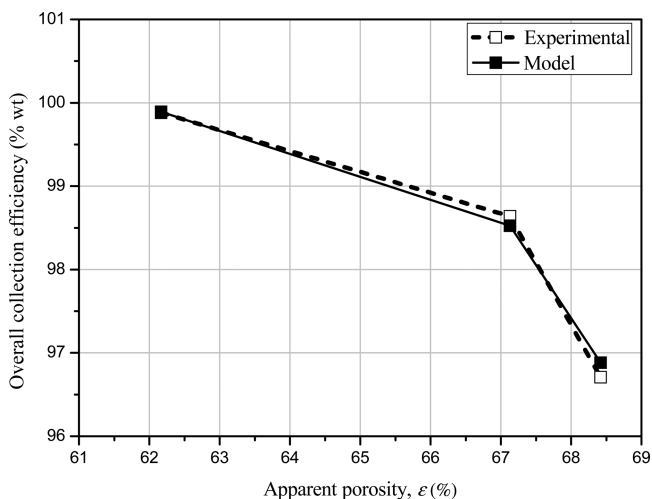
Figure 11. Effect of sample porosity on the overall particle collection efficiency.

between the theoretical (model) and experimental $E_{overall}$ versus ε curves. An increase in porosity is likely to cause a deleterious effect on diffusional mechanism, resulting in the decrease of the collection efficiency with porosity. Similar observation was also made by Freitas et al. and Innocentini et al. who showed that an increase of porosity due to thermal expansion was the reason behind a decrease of capture efficiency of a filter.[56,26] The authors also reported that in countries such as Brazil the flue gas cleaning technologies for sugar cane bagasse boilers require typically an overall efficiency minimum of 97% to meet the particulate matter emission regulations.[26] The overall efficiency of the investigated porous SiC ceramics thus indicates their strong application possibility as filters in nanoparticle separation processes.

IV. CONCLUSION

(1) Cordierite bonded porous SiC ceramics for removal of airborne nanoparticles was successfully prepared by oxide bonding of powder compacts of SiC, Al$_2$O$_3$, and MgO at 1350 °C in air. Samples of varied porosity in a range of 30.1−71.7%

could be synthesized by the variation of petroleum coke pore former volume fraction from 0.23 to 0.76. Stoichiometric formation of cordierite was possible by maintaining the Al_2O_3 to MgO molar ratio of 2:1; the desired amount of silica was obtained by the oxidation of SiC. SEM/EDX test supported formation of cordierite in the bond phase bridging the gap between the contacting SiC particles. Microstructure examination also indicated formation of interconnected pore structure. That the porous ceramics behave like true cellular solids is also confirmed by mechanical property data.

(2) A parabolic relationship between pressure drop/superficial velocity was confirmed through high-quality fitting of experimental data to the Forchheimer's equation. Permeability coefficient values could increase several orders of magnitude depending on the addition of the sacrificial pore former used to create porosity in the ceramic material, indicating that it is possible to tailor this parameter according to the need of a specific application.

(3) The permeability coefficients of the porous SiC ceramic samples with porosity greater than ~48% indicated that the values are well within the typical range of hot aerosol filters.

(4) The Darcian permeability coefficient, k_1, but not the non-Darcian permeability coefficient, k_2, fitted well to the Ergun-like equations for granular media; Based on the relationship between the permeability coefficients obtained by fitting a large number of reported k_1 and k_2 data in a permeability map, equations can be proposed for more reliable prediction for k_2 compared to the prediction made by the Ergun-like equations:

$$k_2 = \exp\left(-\frac{2.57394(1-\varepsilon)^{0.16186}}{\varepsilon^{0.24279}d_p^{0.16186}}\right),$$

based on particle size

$$k_2 = \exp\left(-\frac{2.41044}{\varepsilon^{0.08093}d^{0.16186}}\right), \quad \text{based on pore size}$$

(5) Permeation curves obtained at high temperatures (up to ~750 °C) and high superficial velocities (up to 0.90 m s^{-1}) indicated that resistance to fluid flow increased with temperature mainly because of the increase of the fluid viscosity with temperature. Preliminary analysis of the permeability data for air flow at superficial velocities up to 0.05 m s^{-1} and temperatures up to ~750 °C revealed that pressure drop is mostly governed by viscous effects and Darcy's law is valid for the test conditions, suggesting the possibility of application of porous SiC ceramics as filtering media for typical aerosol filtration processes.

(6) The filtration of nanoparticles (of sizes from 7 to 300 nm) in the SiC filter ceramics had showed that fractional particle collection efficiency decreased with increasing particle size at fixed fluid superficial velocity (0.10 m s^{-1}). The size-selective fractional collection efficiency of the filter ceramics could be described very well by the single-collector efficiency model for granular filters based on classical collection mechanisms. The comparison of experimental results with the calculated collector efficiency showed the predominance of diffusional mechanism in the range studied.

(7) The overall dust collection efficiency measured with the samples of porosity varying from 62 to 68% showed a decreasing trend with porosity, likely because of the deleterious effect of porosity on the diffusional mechanism. The overall efficiency could also be modeled on the basis of the single-

collector size from a range of 19.6−23.4 μm—a range of particle diameter used in the present study—and a very good agreement between the modeled and experimental overall collection efficiency−porosity relations was obtained. The overall efficiency of the investigated SiC samples thus indicates their strong application possibilities in nanoparticle filtration processes.

■ AUTHOR INFORMATION

Corresponding Author
*Tel.: +91-33-24733469/3496 Ext. 3473; Fax: +91-33-24730957. E-mail: omprakash@cgcri.res.in.

Notes
The authors declare no competing financial interest.

■ NOMENCLATURE

a	fitting constant in eq 19
A	filter face area exposed to fluid flow (m^2)
A_S	Happel's parameter
D	diffusion coefficient (m^2 s^{-1})
d_c	average collector diameter (m)
d_{eq}	mean spherical particle diameter (m)
d_{pi}	dust particle size (m)
d_{pore}	average pore size (m)
d_{vs}	Sauter mean diameter of the particle/grain/fiber (m)
E	Young's modulus (GPa)
E_{frac}	fractional collection efficiency
$E_{overall}$	overall collection efficiency
F_o	Forchheimer's number
F_S	slip correction factor
G	acceleration due to gravity (m s^{-2})
K	dimensionless parameter defined in eq 20
k_1	Darcian permeability coefficient (m^2)
k_2	non-Darcian permeability coefficient (m)
k_B	Boltzmann constant (m^2 kg s^{-2} K^{-1})
L	sample thickness (m)
MM_{air}	average molar mass of dry air (kg mol^{-1})
N_{Pe}	Peclet number
N_R	interception parameter
N_{Re}	Reynolds' number
N_{St}	Stokes' number
$N_{St_{eff}}$	effective Stokes' number
P	absolute pressure (kg m^{-1} s^{-2})
P_i	absolute inlet pressure (kg m^{-1} s^{-2})
P_o	absolute outlet pressure (kg m^{-1} s^{-2})
Q	volumetric flow rate of the fluid (m^3 s^{-1})
R^2	correlation coefficient
T	absolute temperature (K)
v_s	fluid velocity (m s^{-1})
v_t	terminal setting velocity (m s^{-1})

Greek Letters

α	thermal expansion coefficient

18370

dx.doi.org/10.1021/ie402876v | *Ind. Eng. Chem. Res.* 2013, 52, 18362−18372

ε apparent porosity (vol %)
η_D single collector efficiency due to diffusion
η_{DI} single collector efficiency due to direct interception
η_E single collector efficiency due to electrophoresis
η_G single collector efficiency due to gravity
η_I single collector efficiency due to inertia
η_T total single collector efficiency
λ mean free path of gas molecules (m)
μ fluid viscosity (kg m^{-1} s^{-1})
ρ fluid density (kg m^{-3})
ρ_p dust particle density (kg m^{-3})
σ flexural strength (MPa)

■ REFERENCES

(1) Peukert, W. High temperature filtration in the process industry. *Filtr. Sep.* **1998**, *35*, 461.

(2) Seville, J. P. K. *Gas cleaning in demanding applications*; Blackie Academic and Professional: London, 1997.

(3) Startin, A.; Elliott, G. Controlling emissions with ceramic filters. *Feature Report: Chem. Eng.* **2009**, *January*, 35 http://www.georgiaair.org/airpermit/downloads/permits/16300035/psd20584/facilitydocs/0109clearedgearticle.pdf.

(4) Moss, K. D. Ceramic filter systems—Controlling furnace emissions with low-density ceramic filters is a crucial part of glass manufacturing. *Ceram. Ind.* **2012**, *162* (6), 23.

(5) Ito, S.; Tanaka, T.; Kawamura, S. Changes in pressure loss and face velocity of ceramic candle filters caused by reverse cleaning in hot coal gas filtration. *Powder Technol.* **1998**, *100*, 32.

(6) Woo, S. K.; Lee, S. K.; Han, I. S.; Seo, D. W.; Park, Y. O. Role of porosity in dust cleaning of silicon carbide ceramic filters. *J. Ceram. Soc. Jpn.* **2001**, *109*, 742.

(7) Kitaoka, S.; Kawashima, N.; Komatsubara, Y.; Yamaguchi, A.; Sujuki, H. Improved filtration performance of continuous alumina fiber-reinforced mullite composites for hot gas cleaning. *J. Am. Ceram. Soc.* **2005**, *88*, 45.

(8) Lupión, M.; Ortiz, F. J. G.; Navarrete, B.; Cortés, V. J. Assessment performance of high-temperature filtering elements. *Fuel* **2010**, *89*, 848.

(9) Simeone, E.; Siedlecki, M.; Nacken, M.; Heidenreich, S.; de Jong, W. High temperature gas filtration with ceramic candles and ashes characterisation during steam–oxygen blown gasification of biomass. *Fuel* **2013**, *108*, 99.

(10) Leibold, H.; Dirks, F.; Rüdinger, V. Particulate emissions from a low incinerator and off-gas cleaning with a new type of ceramic candle filter. *Waste Manage.* **1989**, *9*, 87.

(11) Alonso-Fariñas, B.; Lupion, M.; Rodriguez-Galan, M.; Martinez-Fernandez, J. New candle prototype for hot gas filtration industrial applications. *Fuel* **2013**, *114*, 120.

(12) Pastila, P. H.; Helanti, V.; Nikkila, A. P.; Mantyla, T. A. Effect of crystallization on creep of clay-bonded SiC filters. *Ceram. Eng. Sci. Proc.* **1998**, *19*, 37.

(13) She, J. H.; Deng, Z. Y.; Doni, J. D.; Ohji, T. Oxidation bonding of porous SiC ceramics. *J. Mater. Sci.* **2002**, *37*, 3615.

(14) Chun, Y. S.; Kim, Y. W. Processing and mechanical properties of porous silica-bonded silicon carbide ceramics. *Met. Mater. Int.* **2005**, *11*, 351.

(15) She, J. H.; Ohji, T. Fabrication and characterization of highly porous mullite ceramics. *Mater. Chem. Phys.* **2003**, *80*, 610.

(16) Bardhan, N.; Bhargave, P. In situ reaction sintering of porous mullite bonded SiC. Its mechanical behavior and high temperature application. *Ceram. Eng. Sci. Proc.* **2008**, *29*, 127.

(17) Dey, A.; Kayal, N.; Chakrabarti, O. P. Preparation of mullite bonded porous SiC ceramics by an infiltration technique. *J. Mater. Sci.* **2011**, *46*, 5432.

(18) Liu, S. F.; Zeng, Y. P.; Jiang, D. L. Fabrication and characterization of cordierite-bonded porous SiC ceramics. *Ceram. Int.* **2009**, *35*, 597.

(19) Purchas, D. B., Sutherland, K. *Handbook of Filter Media*; Elsevier Science & Technology Books: Amsterdam, 2002.

(20) Lupion, M.; Alonso-Farinas, B.; Rodriguez-Galan, M.; Navarrete, B. Modelling pressure drop evolution on high temperature filters. *Chem. Eng. Process.* **2013**, *66*, 12.

(21) Howard, C. V. *Statement of Evidence: Particulate Emissions and Health. Proposed Ringaskiddy Waste-to-Energy Facility*, June 2009. Retrieved Aug. 4, 2013 at http://www.cawdrec.com/incineration/CVH.pdf.

(22) Dey, A.; Kayal, N.; Chakrabarti, O. P.; Caldato, R. F.; Innocentini, M. D. M.; Guerra, V. G. Investigations on material and mechanical properties, air-permeation behavior and filtration performance of mullite-bonded porous SiC ceramics. *Int. J. Appl. Ceram. Technol.* **2013**, DOI: 10.1111/ijac.12090.

(23) Innocentini, M. D. M.; Silva, M. G.; Menegazzo, B. A.; Pandolfelli, V. C. Permeability of refractory castables at high temperatures. *J. Am. Ceram. Soc.* **2001**, *84*, 645.

(24) Dey, A.; Kayal, N.; Chakrabarti, O. P.; Chacon, W. S.; Innocentini, M. D. M.; Coury, J. R. Evaluation of air permeation behavior of porous SiC ceramics synthesized by oxidation bonding technique. *Int. J. Appl. Ceram. Technol.* **2012**, DOI: 10.1111/j.1744-7402.2012.02847.x.

(25) Biasetto, L.; Innocentini, M. D. M.; Chacon, W. S.; Corradetti, S.; Carturan, S.; Colombo, P.; Andrighetto, A. Gas permeability of lanthanum oxycarbide targets for the SPES project. *J. Nucl. Mater.* **2013**, *440*, 70.

(26) Innocentini, M. D. M.; Rodrigues, V. P.; Romano, R. C.; Pileggi, R. G.; Silva, G. M.; Coury, J. R. Permeability optimization and performance evaluation of hot aerosol filters made using foam incorporated alumina suspension. *J. Hazard. Mater.* **2009**, *162*, 212.

(27) Innocentini, D. M. D.; Sepulveda, P.; Ortega, F. S. In *Cellular Ceramics: Structure, Manufacturing, Properties and Application*; Scheffler, M., Colombo, P., Eds.; Wiley-VCH: Weinheim, Germany, 2005; pp 313–341.

(28) Scheidegger, A. E. *The physics of flow through porous media*, 3rd ed.; University of Toronto Press: Toronto, 1974.

(29) Innocentini, M. D. M.; Pardo, A. R. F.; Pandolfelli, V. C. Influence of air compressibility on the permeability evaluation of refractory castables. *J. Am. Ceram. Soc.* **2000**, *83*, 1536.

(30) Liu, S.; Zeng, Y. P.; Jiang, D. Effects of CeO$_2$ addition on the properties of cordierite-bonded porous SiC ceramics. *J. Eur. Ceram. Soc.* **2009**, *29*, 1795.

(31) Rice, R. W. Extension of the exponential porosity dependence of strength and elastic moduli. *J. Am. Ceram. Soc.* **1976**, *59*, 536.

(32) Rice, R. W. Comparison of stress concentration versus minimum solid area based mechanical property-porosity relations. *J. Mater. Sci.* **1993**, *28*, 2187.

(33) She, J. H.; Yang, J. F.; Kondo, N.; Ohji, T.; Deng, Z. Y.; Kanzaki, S. High strength porous SiC ceramics by oxidation bonding technique. *J. Am. Ceram. Soc.* **2002**, *85*, 2852.

(34) Magdeski, J. S. The porosity dependence of mechanical properties of sintered alumina. *J. UCTM* **2010**, *45*, 143.

(35) Knudsen, F. P. Dependence of mechanical strength of brittle crystalline specimens on porosity and grain size. *J. Am. Ceram. Soc.* **1959**, *42*, 376.

(36) Ohzawa, Y.; Nomura, K.; Sugiyama, K. Relation between porosity and pore size or pressure drop of fibrous SiC filter prepared from carbonized cellulose-powder performs. *Mat. Sci. Eng., A* **1998**, *255*, 33.

(37) Sepulveda, P.; Ortega, F. S.; Innocentini, M. D. M.; Pandolfelli, V. C. Properties of highly porous hydroxyapatite obtained by the gelcasting of foams. *J. Am. Ceram. Soc.* **2000**, *83*, 3021.

(38) Kanaoka, C.; Amornkitbamrung, M. Effect of filter permeability on the release of captured dust from a rigid ceramic filter surface. *Powder Technol.* **2001**, *118*, 113.

(39) Ergun, S. Fluid flow through packed columns. *Chem. Eng. Prog.* **1952**, *48*, 89.

(40) Meyer, B. A.; Smith, D. W. Flow through Porous Media: Comparison of Consolidated and Unconsolidated Material. *Ind. Eng. Chem. Fundam.* **1985**, *24*, 360.

(41) Narayanaswamy, G.; Sharma, M. M.; Pope, G. A. Effect of heterogeneity on the non-Darcy flow coefficient. *SPE Reservoir Eval. Eng.* **1999**, *2* (3), 296.

(42) Belhaj, H. A.; Agha, K. R.; Nouri, A. M.; Butt, S. D.; Islam, M. R. *Numerical and Experimental Modeling of Non-Darcy Flow in Porous Media.* Paper SPE 81097 presented at the Latin American and Caribbean Petroleum Engineering Conference, Port-of-Spain, Trinidad and Tobago, Apr. 27–30, 2003; DOI: 10.2118/81037-MS.

(43) Biasetto, L.; Colombo, P.; Innocentini, M. D. M.; Mullens, S. Gas permeability of microcellular ceramic foams. *Ind. Eng. Chem. Res.* **2007**, *46*, 3366.

(44) Jo, Y. M.; Hutchison, R. B.; Raper, J. A. Characterization of ceramic composite membrane filters for hot gas cleaning. *Powder Technol.* **1997**, *91*, 55.

(45) Barg, S.; Innocentini, M. D. M.; Meloni, R. V.; Chacon, W. S.; Wang, H.; Koch, D.; Grathwohl, G. Physical and high-temperature permeation features of double-layered cellular filtering membranes prepared via freeze casting of emulsified powder suspensions. *J. Membr. Sci.* **2011**, *383*, 35.

(46) Lupión, M.; Ortiz, F. J. G.; Navarrete, B.; Cortés, V. J. Assessment performance of high-temperature filtering elements. *Fuel* **2010**, *89*, 848.

(47) Tien, C.; Ramarao, B. V. *Granular Filtration of Aerosols and Hydrosols.* 2nd ed.; Elsevier: Boston, MA, USA, 1989.

(48) Coury, J. R. *Electrostatic effects in granular bed filtration of gases.* Ph.D. Thesis, University of Cambridge, Cambridge, U.K., 1983.

(49) Yoshida, H.; Tien, C. A new correlation of the initial collection efficiency of granular aerosol filtration. *AIChE J.* **1985**, *31*, 1752.

(50) Allen, M. D.; Raabe, O. G. Slip correction measurements of spherical solid aerosol particles in an improved Millikan apparatus. *Aerosol Sci. Technol.* **1985**, *4*, 269.

(51) Jung, Y.; Walata, S. A.; Tien, C. Experimental determination of the initial collection efficiency of granular beds in the inertial-impaction-dominated region. *Aerosol Sci. Technol.* **1989**, *11*, 168.

(52) Paretsky, L.; Theodore, L.; Pfeffer, R.; Squires, A. M. Panel bed filters for simultaneous removal of fly ash and sulphur dioxide. 2: Filtration of dilute aerosols by sand beds. *J. Air Pollut. Control Assoc.* **1971**, *21*, 204.

(53) Coury, J. R.; Thambimuthu, K. V.; Clift, R. Capture and rebound of dust in granular bed filters. *Powder Technol.* **1987**, *50*, 254.

(54) Hinds, W. C. Aerosol technology: Properties. In *Behavior and Measurement of Airborne Particles*, 2nd ed.; John Wiley & Sons: New York, 1999.

(55) Brown, R. *Air Filtration: An Integrated Approach to the Theory and Application of Fibrous Filters*; Pergamon Press: Oxford, U.K., 1993.

(56) Freitas, N. L.; Gonçalves, J. A. S.; Innocentini, M. D. M.; Coury, J. R. Development of a double-layered ceramic filter for aerosol filtration at high-temperatures: The filter collection efficiency. *J. Hazard. Mater.* **2006**, *136*, 747.